Environmental Science & Technology

Article

pubs.acs.org/est

Near-Field Characterization of Methane Emission Variability from a Compressor Station Using a Model Aircraft

Brian J. Nathan,[†] Levi M. Golston,[‡,§] Anthony S. O'Brien,[‡,§] Kevin Ross,[‡,§] William A. Harrison,[†] Lei Tao,[‡,§] David J. Lary,[†] Derek R. Johnson,[∥] April N. Covington,[∥] Nigel N. Clark,[∥] and Mark A. Zondlo*[,‡,§]

[†]William B. Hanson Center for Space Sciences, University of Texas at Dallas, 800 West Campbell Road, Richardson, Texas 75080, United States

[‡]Department of Civil and Environmental Engineering, Princeton University, EQuad E-209A, Princeton, New Jersey 08544, United States

[§]Center for Mid-Infrared Technologies for Health and the Environment, Princeton University, 70 Prospect Ave., Princeton, New Jersey 08540, United States

[∥]Center for Alternative Fuels, Engines, and Emissions, West Virginia University, 395 Evansdale Drive, Morgantown, West Virginia 26505, United States

Supporting Information

ABSTRACT: A model aircraft equipped with a custom laser-based, open-path methane sensor was deployed around a natural gas compressor station to quantify the methane leak rate and its variability at a compressor station in the Barnett Shale. The open-path, laser-based sensor provides fast (10 Hz) and precise (0.1 ppmv) measurements of methane in a compact package while the remote control aircraft provides nimble and safe operation around a local source. Emission rates were measured from 22 flights over a one-week period. Mean emission rates of 14 ± 8 g CH_4 s^{-1} (7.4 ± 4.2 g CH_4 s^{-1} median) from the station were observed or approximately 0.02% of the station throughput. Significant variability in emission rates (0.3−73 g CH_4 s^{-1} range) was observed on time scales of hours to days, and plumes showed high spatial variability in the horizontal and vertical dimensions. Given the high spatiotemporal variability of emissions, individual measurements taken over short durations and from ground-based platforms should be used with caution when examining compressor station emissions. More generally, our results demonstrate the unique advantages and challenges of platforms like small unmanned aerial vehicles for quantifying local emission sources to the atmosphere.

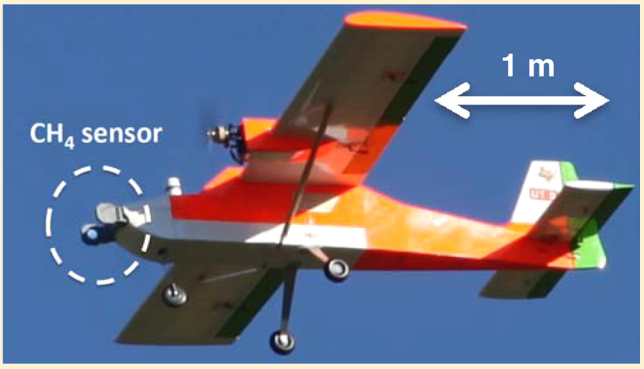

INTRODUCTION

Methane (CH_4) emission inventories from the natural gas supply chain using bottom-up approaches often have high uncertainties and are inconsistent with top-down approaches.[1] The representativeness of a relatively small number of samples is a concern, particularly for the case of a highly skewed distribution of emissions.[1−3] The sampling methods themselves for such localized sources also have significant uncertainties.[1−4] Sampling challenges include limited site access arising from property rights, topography, physical obstructions (e.g., trees), or the road network. Turbulence, particularly in unstable conditions, will tend to loft any emissions to heights well above ground-based measurement sites or vehicle-based platforms. Airborne-based platforms such as manned light aircraft effectively capture lofted plumes[5−7] but cannot be flown at very low altitudes or close to sources due to public safety and property damage concerns. Finally, significant temporal variability of individual sources may not be captured in a single measurement regardless of the method.

Small unmanned aerial systems (sUAS) are a rapidly maturing technology that can readily sample the lowermost boundary layer around a local emission source such as a compressor station at high spatial resolution. Unfortunately, most commercial and even research-based trace gas sensors are too heavy, power hungry, or large to fit on sUAS that have payloads of a few ∼ kg in mass, few L in volume, and power consumption of <100 W. Open-path, laser-based trace gas sensors can provide precise and fast measurements while fitting the payload constraints of remote control aircraft or sUAS.[8]

Received: February 9, 2015
Revised: May 8, 2015
Accepted: May 8, 2015
Published: May 26, 2015

DOI: 10.1021/acs.est.5b00705
Environ. Sci. Technol. 2015, 49, 7896−7903

However, there remain open questions on how to deploy such systems for scientific studies, how the emissions derived from such an airborne-based platform compare with more standard approaches on the ground, and the need for additional vertical observational capabilities when quantifying emission rates.

To these ends, a custom, compact, laser-based methane sensor was developed and coupled to a remote control aircraft with a 3 m wingspan. The system was flown around a compressor station to quantify fugitive methane emissions as part of the Environmental Defense Fund's Barnett Coordinated Campaign in October 2013 in Texas.[9] The spatial and temporal variability of the plumes, fugitive methane emission rates from the compressor station, comparison to ground-based methods, and protocols for sampling more generally with such a system will be discussed.

EXPERIMENTAL METHODS

The Environmental Defense Fund's Barnett Coordinated Campaign occurred in October 2013 in the Barnett Shale with a suite of airborne and ground-based measurements.[9] The measurements in this study were focused on a representative natural gas compressor station located in the Barnett Shale. The site was comprised of equipment from five different operators. A total of 22 flights were conducted from October 22–29, 2013, around the natural gas compressor station, in addition to test flights at a separate location. Relevant measurements at this site in the Barnett Coordinated Campaign included a detailed leak and loss audit performed by West Virginia University (WVU) on all equipment associated with one of the five site operators. The detailed audit occurred on October 16th and 17th with repeated measurements during sUAS flights on October 25th.[10] In addition, a mobile laboratory measurement of CH_4 was conducted on October 31, 2013, by the University of Houston.[4]

Experimental Section. The methane sensor consisted of a fiberized 1651 nm distributed feedback laser (Norcada, Inc.) coupled to pair of 5.1 cm diameter spherical mirrors separated by 20 cm. The mirrors made a Herriott-style, multiple pass optical cell with a total optical path length of 20 m (100 passes). Light was collected by an extended wavelength InGaAs detector (Teledyne-Judson). Wavelength modulation spectroscopy was implemented with the laser injection current ramped in a sawtooth function at 50 Hz (with a 12% duty cycle below threshold to acquire a laser-free background) and a sinusoidal modulation superimposed on the sawtooth ramp at a frequency of f = 50 kHz. The second harmonic ($2f$) of the demodulated photodetector signal was used for high-sensitivity detection. Data were coaveraged to 10 Hz and saved to the single-board computer running LabVIEW software (National Instruments). To be consistent with the geolocation data, the CH_4 data were further averaged to 1 s and synchronized with the GPS pulse-per-second signal. A linear least-squares fit of a stored reference spectrum to the ambient signal was used to determine the concentration. The stored reference spectrum was taken within 15 min of flight at ambient temperatures and pressures to account for slight variations in ambient conditions between each flight. Deviations of temperature (±2 K) and pressure (−18 hPa) from the takeoff conditions were neglected in the spectral fits. HITRAN simulations show this range of conditions impacted the peak absorption of the methane line by less than 1%. The laser current and temperature controller (Wavelength Electronics, Inc.), digital-analog boards, lock-in amplifier, and single board computer were located in the fuselage of the aircraft. The optical head was placed ∼20 cm in front of the nose of the aircraft to avoid disturbances from the winds and electric motors of the aircraft. Figure 1 shows a photograph of the sensor. The sensor had a mass of 3.1 kg, consumed 25 W of power, and had a precision of 0.1 ppmv at 1 Hz. Precision was determined by enclosing the optical sensor head at ambient conditions in the laboratory and analyzing the Allan deviation. Long-term drift was less than the 1 Hz precision at time scales up to 600 s, a time scale longer than any flight.

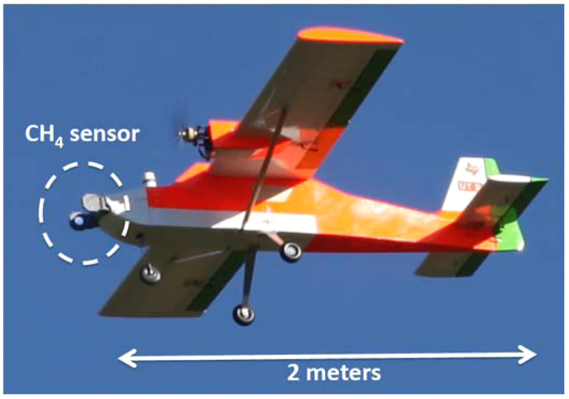

Figure 1. Photograph of the remote control aircraft with the Princeton open-path CH_4 sensor on the front.

The remote control aircraft was a modified AMR Payload Master 100. It was adapted to a dual-motor design with each motor powered by a 7.5 horsepower, 50 cm^3 equivalent electric engine. The motors were powered by two Hyperion 5400 mAh batteries with the sensor operated by a separate but identical battery for safety concerns. Mounted above the nose of the plane was a New Mountain Weather Station (0.3 kg) that measured ambient air temperature, pressure, wind speed, and direction. A GPS unit collected the plane's position and time, from which the ground speed and direction were derived. The wind speed and direction from the aircraft were inconsistent with a nearby weather station at the airport upon flight takeoff and thus were not used in the analyses. Average flight times were 409 s (min. 256 s; max. 541 s) at ground speeds of 15–30 m s^{-1}. The compressor station was typically flown around 4–8 times per flight. Flight operations occurred in daytime due to visibility concerns, and most flights occurred in the late morning to late afternoon (see Supporting Information Table SM 1). Per hobbyist regulations, the maximum flight ceiling was limited to 122 magl (meters above ground level). All landowners granted prior written permission to fly over and around the site.

Wind speed and direction (MetOne WS 010 C-1, WD 020 C-1) were measured every 1 s from a nearby Texas Commission on Environmental Quality (TCEQ) field site operated by URS Corp. for the North Texas Commission. The wind was measured on a tower at an elevation of 10 m above the ground. The tower was located 59 m southwest (237°) of the end of the runway and 310 m northwest (331°) of the central exhaust stack of the compressor station. The wind data were coaveraged to 5 min intervals. The accuracies of the wind speed and direction were ±0.1 m s^{-1} and ±3°, respectively.

Based on satellite images there are at least six total engines at the site (owned by a total of five operators). The single operator audited by WVU included two Caterpillar G3612

DOI: 10.1021/acs.est.5b00705
Environ. Sci. Technol. 2015, 49, 7896–7903

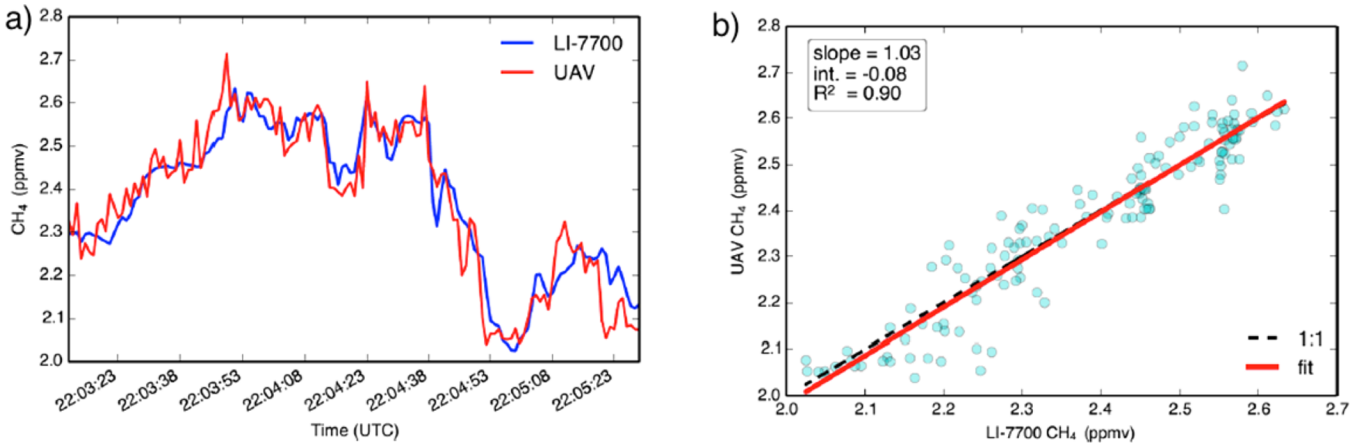

Figure 2. a) Side-by-side intercomparison of the laser-based CH_4 sensor on aircraft (red) and LICOR LI-7700 (blue). b) regression plot of the same data showing 3% agreement between the instruments.

rated at 3785 hp. During the audit, only one of the two engines by this operator was operational and did so continuously (24 h/day) at 80% load or 169 million cubic feet (MMcf) d^{-1}. The operational behaviors of the other engines were not known. By applying the same operational status (50%), load (80%), and engine size (3785 hP) to the four other engines, this station would have moved 507 MMcf d^{-1} of natural gas. Based upon EIA transmission data, approximately 0.06 MMcf of natural gas is transmitted per day per horsepower along a pipeline.[11] If the other operators had the same engines as the audited operator, the maximum throughput for the site would be 1363 MMcf d^{-1}. Average compressor stations move 700 MMcf d^{-1}, so the compressor station of interest is likely representative of a typical compressor station in terms of throughput. The exact location and audited operator of the compressor station are confidential based upon a nondisclosure agreement with the Environmental Defense Fund.

Methods. Because the model aircraft flew around the compressor station, data were transformed onto a polar coordinate system (r, θ) using the central exhaust stack from the compressor station as the origin. A new variable was defined as $\phi = \theta - \theta_{MET}$, representing the difference between the prevailing wind direction (θ_{MET}) and the radius vector from the origin. Data were considered downwind if $-45° < \phi < 45°$. To remove biases from nearby sources (wells, condensate tanks), the data were further restricted to $r < 295$ m. Data on the upwind side at CH_4 mixing ratios less than the sum of the mean and 3σ precision (σ = 0.1 ppmv) were set as the background[5] to avoid the influence of CH_4 plumes upwind of the compressor station.

To calculate an emission rate, a two-dimensional interpolation plane (referred to as the "flux surface") was defined to be perpendicular to the prevailing wind direction. The average latitude and longitude of the filtered data were used as the midpoint for the flux surface. Specifying the flux surface with this method minimizes the distance that each measurement must be projected to reach the two-dimensional interpolation surface. A Kriging interpolation[5] scheme was then applied to the nonuniformly spaced data onto a rectangular 19 × 19 grid. For each flight, estimates of the expected value and variances of downwind CH_4, pressure, temperature, and windspeed were produced using the software package "EasyKrig 3.0" (http://globec.whoi.edu/software/kriging/easy_krig/easy_krig.html). This method operates by minimizing the variance of the error of the estimation based on a theoretical system of linear equations. The coefficients for these equations are found by producing a covariance function that quantifies the correlation between measured data at two sampling locations.[12] The covariance function used a general exponential Bessel relationship. The grid parameters for each analysis depended on the flight pattern with the extents set based on the length of the flux surface and altitude range covered by the aircraft. The grid resolution varied from 1.2 to 7.2 m in the vertical dimension and 11.6 to 24.4 m in the horizontal dimension. The average downwind distance from the flux surface to origin was 170 m.

After isolating and Kriging the downwind data, the emission rate was calculated using an integral over the flux surface:[5]

$$F(CH_4) = \int\int \nu(z)\sin(\alpha)n\cdot(u_d(x,z) - u_{bg})dxdz \quad (1)$$

where ν is the mean wind speed, α is the angle of the wind velocity relative to the flux surface, n(z) the density of air calculated using the ideal gas law with Kriged temperature and pressure data, $u_d(x,z)$ is the downwind CH_4 mixing ratio, and u_{bg} is the background mixing ratio. Equation 1 is discretized to be the sum over the 19 × 19 Kriging grid, with dx and dz being the horizontal and vertical resolution of the grid, respectively. The Kriged variances in each of these variables are propagated through eq 1 to produce an uncertainty estimate, assuming negligible uncertainty in the grid parameters dx and dz.

As a complementary analysis to the Kriging interpolation, a nonlinear optimization was performed with a Gaussian plume equation to find the stack emission rate that best correlated with the observations. Here, the same polar coordinate system was used with a narrower definition of "downwind" as before (±23°), which is a safe range for pollutants emitted within 1 h.[13] The function calculating the Gaussian plume used the standard equation,

$$C(x,y,z) = \frac{Q}{2\pi\bar{u}\sigma_y\sigma_z}\exp\left(\frac{-y^2}{2\sigma_y^2}\right)\left[\exp\left(\frac{-(z-h)^2}{2\sigma_z^2}\right) + \exp\left(\frac{-(z+h)^2}{2\sigma_z^2}\right)\right] \quad (2)$$

where C is the concentration, x is the downwind coordinate, y is the cross-wind coordinate, z is the altitude above ground level, h is the stack height, $\bar{u}$ is the average wind speed, σ_y is the

DOI: 10.1021/acs.est.5b00705
Environ. Sci. Technol. 2015, 49, 7896−7903

standard deviation in the y-direction, σ_z is the standard deviation in the z-direction, and Q is the emission rate. Some of these values are influenced by other variables such that our predictor function was actually of the form:

$$f(Q) = C(x, y, z) = f(Q; \bar{u}, h, \text{class}, p, mw, T_a, T_s, d_s, C_p, P_a, P_s, \nu_s, x, y, z) \quad (3)$$

where class is the stability class of the atmosphere from the Pasquill-Gifford scale,[14] p is the wind profile exponent, mw is the molecular weight, T_a is the ambient temperature, T_s is the stack temperature, d_s is the stack tip diameter, C_p is the specific heat of the effluent, P_a is ambient pressure, and ν_s is the stack tip velocity. All of these extra variables relate to the variables in eq 3 based on the EPA ISC3 dispersion models.[15]

RESULTS AND DISCUSSION

The aircraft CH_4 sensor, and a ground-based LICOR LI-7700 for intercomparisons, were calibrated before and after the campaign with a NOAA ESRL/GMD/WMO standard of 1871.26 (±0.3) ppbv and also with a certified mixture of 5.05 ppmv (±5%) CH_4 in air (Air Liquide). While the LI-7700 has excellent field stability better than 0.02 ppmv,[16] it was unclear how the aircraft-based sensor would maintain its calibration on the aircraft and in the field. To this end, both sensors were placed side-by-side for a short duration prior to takeoff before most flights. Figure 2a shows a timeseries of both the LICOR 7700 and the aircraft methane sensors on the ground (separated by 2 m) immediately prior to aircraft taxi. The two measurements follow one another very closely with significant CH_4 variability. Figure 2b is a linear regression of the same data with excellent agreement (<3%) at the elevated mixing ratios observed in this study. Note that some of the differences may be related to the two instruments sampling different air masses as the site exhibits high variability in CH_4. Based upon the short-term noise, reproducibility, calibrations, and intercomparison data, the uncertainty of airborne CH_4 mixing ratios is estimated to be ±10%. Note that while this accuracy is insufficient for free troposphere measurement requirements,[5−7,17] the enhancements above background near the compressor station greatly exceeded this level of uncertainty in the airborne-based measurement. Further, detecting enhancements above background levels are more dependent upon sensor precision (0.1 ppmv) than the stated accuracy.

Figure 3 shows a plot of a representative time series when transecting well-defined plumes in the air. Note that the highest plumes show enhancements more than twice the ambient background signal (typically ∼2.2 ppmv at this location and time). Also note that the largest plumes are very narrow (1−2 s duration or 10−30 m) horizontally in space with the aircraft transecting the plumes on the order of a second. Overall, the horizontal plume widths for the highest concentration plumes on all flights were on the 10−50 m scale. The open-path configuration provides the fast time response that is critical for identifying the plumes even at the relatively slow speeds of a model aircraft (compared to a manned aircraft).

The compressor station is not a point source, as other CH_4 sources exist besides the compressor station exhaust stacks. Indeed, most flights indicated more than a single, well-defined plume. To quantify the flux rate, the Kriging interpolation was used on the downwind flight data. Flight 26 will be used to demonstrate a representative case. Figure 4a shows the flight track−colored by CH_4 mixing ratios−around the compressor station. Note that large CH_4 mixing ratios are observed in other locations well downwind of the compressor station. There were other sources of natural gas infrastructure in this region including wells, condensate tanks, and pipelines. For these reasons, the analyses are restricted to those locations immediately downwind of the compressor station. Figure 4b shows the polar coordinate data within the downwind criteria and the location of the averaged cross-section flux surface used in the Kriging interpolation. Figure 4c shows the vertical distribution of the flight (ground level was ∼200 m) relative to the flux surface. Finally, Figure 4d shows the interpolation results on the flux surface corresponding to an emission rate across this surface of 16 ± 3 g CH_4 s^{-1}. The statistical uncertainty derived from the Kriging interpolation fit, as discussed later, is not representative of the total uncertainty in the measurement. Note that several areas of enhancement are identified, both lofted above the surface and near the ground level.

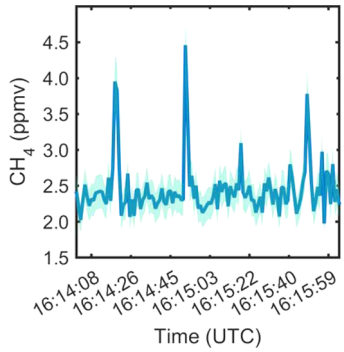

Figure 3. Time series of 1 Hz data in-flight at an altitude of 57 m while crossing three large plumes (flight 23). The uncertainty of the measurement is included in the lighter blue color.

Table S1 in the Supporting Information shows the measured fluxes for all flights with valid measurements (at least two passes around the station) and their Kriged uncertainties (which again are not the total uncertainties, see below). The wind speed and direction shown in Supporting Information Table S1 includes 10 min before and after the flight to assess the larger meteorological conditions on the same spatial scale (∼1 km) as the flight plan (e.g., 1 m s^{-1} wind at 10 min = 600 m). The median emission rate measured over all 22 valid flights was 7.4 g CH_4 s^{-1} (mean 14 g CH_4 s^{-1}) from this compressor station. Large variability was observed within the airborne data set with the highest emission rate of 73 g CH_4 s^{-1} and a low of 0.3 g CH_4 s^{-1}.

It is unclear how much of the variability is due to real changes in emission rates, atmospheric variability, and flight sampling issues. To estimate these effects, pairs of flights adjacent in time and with similar weather conditions were examined. For example, the shortest duration between flights was on Oct. 29 (flights 30, 31) with 1950 s (33 min.), and this pair of flights yielded emission rates of 2.6 and 4.5 g CH_4 s^{-1}. For both flights, the mean wind speed was high (5.8 ± 0.5, 5.5 ± 0.6 m s^{-1}), from nearly the same direction (172 ± 1°, 170 ± 4°), and showed little variability within each flight in either speed or direction. Because flights encircle the compressor station, the absolute wind direction between flights does not matter if all emissions are captured equally well. The more

DOI: 10.1021/acs.est.5b00705
Environ. Sci. Technol. 2015, 49, 7896−7903

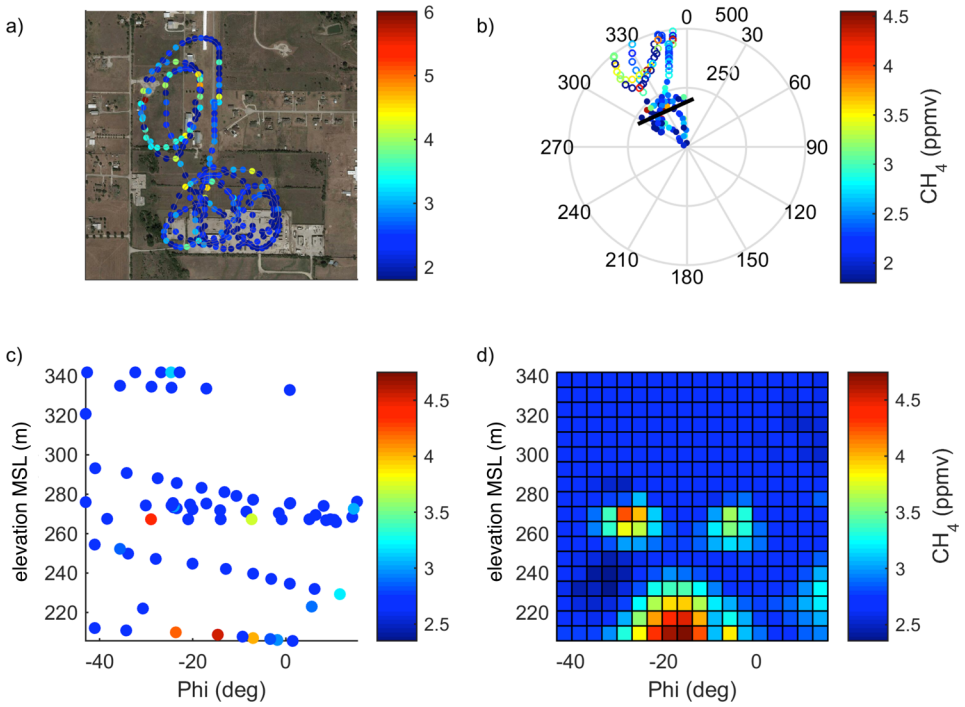

Figure 4. (a) Plot of flight track around the compressor station (lower middle) for Flight 26; (b) Data meeting downwind criteria from the center of the compressor station, showing the filtered near-field points (solid circles), far-field points (open circles) and the modeled flux plane (solid line); (c) Polar coordinate representation of the flux plane used for the Kriging interpolation; (d) Kriged data for Flight 26 on the polar coordinate representation of the flux plane. For reference, ground altitude above mean sea level (MSL) was 205 ± 5 m.

relevant parameter within a flight is the variability of the wind direction. If the wind is changing direction significantly during a flight, the aircraft may over or under sample a plume relative to one being more constant in position. There were six pairs of flights where the time between flights was less than 1 h (3600 s) and the wind direction variability around each flight was <20°. Of these, five pairs had mean emission rates that were clearly above zero (pair mean >1.7 g CH_4 s^{-1}, justified later), and the average relative uncertainty with respect to the mean was ±43%. For the remaining pair (flights 28, 29) where an emission rate was close to zero (2.1 and 0.3 g CH_4 s^{-1}), an absolute uncertainty of the methodology of ±1 g CH_4 s^{-1} can be estimated. By combining these values, the uncertainty due to flight sampling and atmospheric conditions based upon reproducibility is estimated at ± (43% + 1) g CH_4 s^{-1}. The estimate is based upon the assumption that emissions did not change within an hour. While sampling representativeness and atmospheric variability certainly influence the variability observed in Supporting Information Table S1, the range of variability observed throughout all 22 flights is much larger than this uncertainty estimate, suggesting that temporal variations in compressor station emission rates need further investigation.

Statistical Uncertainty Analyses. In a statistical sense, the interpolated downwind methane concentration was the largest source in the flux error analyses. The downwind flux calculation required an interpolated map in areas where the flight did not sample. Following Mays et al.,[5] the variance of the Kriged results at each grid point was assumed to be representative of the total uncertainty of the CH_4 mixing ratio. The measurement error of ±10% and the Kriged variance at the measurement points are comparable, and both are much smaller than the enhancements above the background when in a plume. Therefore, the standard deviation of the Kriged results yields an uncertainty estimate for each flight. This relative error term corresponded to 46% on average.

Another source of uncertainty is the flux area plane for the Kriging interpolation, both in the selection of a grid size and its location. The 19 × 19 Kriging grid resolution was chosen to be consistent with the typical scales of individual plumes (10−30 m). To assess the sensitivity of the flux estimate to this resolution, we calculated the estimated emission rate for three flights with representative emissions rates on three different days (Flights 23, 26, and 33) with grid resolutions of 19 × 19, 10 × 10, and 40 × 40 (cf. a typical flux plane was ∼370 m horizontal by 120 m vertical). Changing the grid resolution by a factor of 2 in either direction resulted in a 4% absolute change in emission rate. For Flights 20 and 33, the estimate increased at larger grid size, while for Flight 26 the estimate decreased, indicating that the resolution grid size does not significantly bias the interpolated emission rates. Select interpolation schemes were also tested on Flight 23 including Gaussian-linear, Gaussian-cosine, linear and exponential and no significant differences (<5%) were observed compared to the exponential-bessel variogram selected in the analyses.

The uncertainties in the distance of the flux plane relative to the origin directly correlate with the flux for a constant grid resolution (i.e., larger grid sizes, d*x*, at further distances would result in a larger flux). The flux plane was defined by minimizing the distance between each data point and the flux plane itself. With the average radial distance away from the flux plane for all points at ±30 m out of a mean radial distance of 170 m, this corresponds to an uncertainty of ±18% in the measured fluxes.

Uncertainties in the mixing ratio measurement itself (±10%) and in the wind speed (±0.5 m s^{-1}) would directly propagate to the uncertainty of the emission rates. For the wind speed, the

DOI: 10.1021/acs.est.5b00705
Environ. Sci. Technol. 2015, 49, 7896−7903

larger uncertainty is applying the wind velocity from the meteorological tower to the much different location of the aircraft. Because the flight sampling spanned minutes and the terrain was largely flat in the local area (<1% gradient), individual eddies and turbulence in the wind would be averaged out in the analyses even if using aircraft data. It is impossible to quantify this uncertainty without aircraft measurements, however the mean flight duration (409 s) and wind mean speed of 3.8 ± 0.3 m s^{-1} correspond to a length scale of 1.6 km, which is comparable to the spatial scale of the flight paths around the compressor station. The uncertainty in the measured wind speed (0.5 m s^{-1}) plus the mean atmospheric variability of the speed during the flight (σ = 0.3 m s^{-1}) yields a combined uncertainty of ±21%.

By assuming that the errors from Kriging variances (46%), grid resolution (4%), interpolation scheme (5%), CH_4 mixing ratio (10%), and wind speed (21%) are Gaussian in nature, the overall statistical uncertainty of the emission rate is ±55%. For the median emission rate of 7.4 g CH_4 s^{-1}, the uncertainty derived from the statistical analyses (±55% or ±4.1 g CH_4 s^{-1}) is comparable to those estimated from the field-derived estimates (4.2 g CH_4 s^{-1}). The agreement between these estimates also suggests that emissions less than 1.7 g CH_4 s^{-1} are indistinguishable from zero in this technique. Only two flights out of 22 are statistically insignificant from zero emissions by this criterion. Because these uncertainty estimates are larger than the variability observed within and between days, significant temporal variability of the compressor station emissions is occurring at time scales greater than 1 h.

Gaussian Plume Comparison. As one further check on the data, the Kriging data fluxes were compared with a Gaussian plume model. It was determined that a Gaussian single-plume model was not ideal for creating estimates from most of the airborne-gathered data sets at this site, mostly because of the restrictions of the model. Like all basic Gaussian plumes, this one assumed that there were constant and continuous emissions creating a steady-state system, pollutant concentrations were normally distributed, and the terrain was relatively flat. As with the Kriging analysis, it also assumed that the effluent was not being degraded through chemical reactions, and the wind speed was constant in time. Additional uncertainties came from the measurement sensor, as already discussed, and uncertainties from the estimates of the non-Q parameters of eqs 2 and 3, as explained in the Supporting Information. The largest and most problematic assumption for these in-flight data sets, though, was that there would be one central plume.

Although the point source approximation is appropriate for most source inversion studies, the emissions from other locations within the compressor station besides the central exhaust stack did significantly hinder the single-plume-model approach for our gathered data sets. An ideal scenario would have a steady-state plume captured in the 45° cone (±23°) centered at the average downwind direction from the origin point at the main engine's building. In very few flights, however, was a central plume detected, and in no flights was a central plume the only source of in-flight enhancements. For example, Flight 25 had an apparent plume almost directly downwind, but the highest detected concentration occurred at 37° (outside the narrow "downwind" central cone) and there was another apparent plume at ∼210°. These, along with a few other enhancements, all led to a higher concentration outside of the central downwind cone than in it.

The flight that best demonstrates the Gaussian plume model's variability for near-field aerial measurements is Flight 22. Figure 5 shows the Kriged interpolation for this flight. The

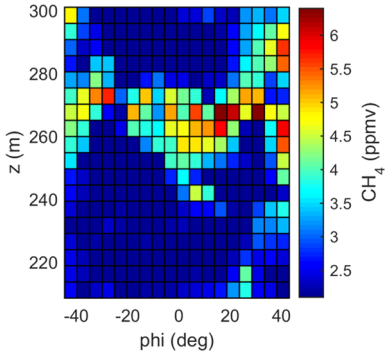

Figure 5. Kriged interpolation from Flight 22 used in the Gaussian plume analyses. For this flight, this represents a flux plane with a midpoint 153 m from station center and a horizontal length of 314 m.

largest group of near-field enhancements captured in-flight are nearly symmetric about the downwind axis. For this flight, the model converged to an emission rate of 23 (17−31) g CH_4 s^{-1}, where the uncertainty range of the model was calculated as explained in the Supporting Information and is independent of the bias from an elevated background. This number compares favorably with the estimate from the Kriging interpolation of 33 ± 10 g CH_4 s^{-1} and shows that this may still be a viable methodology for analysis of aircraft-acquired measurements from a true point source emitter. Future studies may also benefit from optimizing a more refined model such as a segmented Gaussian plume[18] or a Gaussian puff.[19]

Comparison to Other Methods. Two additional and independent measurements of CH_4 emission rates were taken at this compressor station during the campaign. The first measurement used the University of Houston's (UH) mobile laboratory[4] to transect the plume downwind of the site. The UH mobile laboratory measured the site on October 31, 2013, and calculated an emission rate of 5.8 (−3.7, +15.9 at 95% confidence interval) g CH_4 s^{-1} using the EPA AERMOD model. The second measurement was conducted by West Virginia University and included a detailed leak and loss audit of all equipment associated with one of the site operators. The WVU measurements included the leaking components, compressor vents, engine crankcase vents, engine exhaust, and other associated equipment. The detailed audits were performed on October 16th and 17th with repeated measurements during the remote control aircraft flights of October 25th but day-to-day variability was not assessed. The WVU group measured a total emission rate of 5.8 g CH_4 s^{-1} (3.4 g CH_4 s^{-1} from the exhaust stack alone) from one engine operator.

Both of these independent measurements are broadly consistent, though lower, than the mean airborne-based emission rate of 14 (±8) g CH_4 s^{-1}. Given the large temporal variability of CH_4 emissions on time scales of hours to days in the present study, it is difficult to compare measurements taken at different times and over different durations. However, there are probable reasons why the aircraft-derived emissions are higher than those derived from the mobile laboratory or the leak audit. Lofted emissions from the compressor engine exhaust (60% of the total emissions from the leak audit measurements) may not be sampled by the mobile laboratory

DOI: 10.1021/acs.est.5b00705
Environ. Sci. Technol. 2015, 49, 7896−7903

even under stable conditions. The leak audit only was able to sample two of the six engines that operated at this site, and it seems probable that other engines were operating at some capacity. Regardless, the consistency between three vastly different measurement approaches provides confidence in the validity of the remote-controlled aircraft approach, though again potential temporal variations in emission rates make direct comparisons difficult.

■ ATMOSPHERIC IMPLICATIONS

Methane emissions from a compressor station were successfully quantified by merging the new technologies of remote control aircraft with compact, open-path laser-based sensors. Field results show that plumes from compressor stations are often lofted and are very localized in space. A mean emissions rate of 14 (±8) g CH_4 s^{-1} was calculated from a typical compressor station in the Barnett Shale. Emissions showed high variability on time scales of hours to days, ranging from 0 to 73 (±40) g CH_4 s^{-1}. While the relative median CH_4 emission rate is small compared to the estimated total CH_4 throughput of the compressor station (0.02%), the temporal distribution of fugitive CH_4 emission rates from compressor stations needs further study. One-time measurements of a compressor station by any method—vehicle, detailed leak detection, or airborne-based—should be used with caution if the significant variability observed in this study is representative of other compressor stations.

More generally, this study shows that platforms like sUAS are well-suited to quantify emissions from local sources but also require their own unique sensor and sampling considerations. While the high agility of such aircraft to isolate an individual source helps to minimize the influences of nearby sources, sampling near emission sources requires representative and often dense spatial sampling. An autopilot system with a preprogrammed and systematic flight pattern that samples at uniform density in the vertical is highly recommended. There are likely biases in quantifying near-field emissions with aircraft due to the plume changing positions over the duration in which the aircraft completes the flight plan. There are also challenges of locating a spatially small plume at such close distances to the source. On the other hand, the sensor precision/sensitivity demands are relaxed (higher concentrations with less dilution, stronger enhancement above background). Remote control aircraft or sUAS provide unique tools for quantifying local source emissions of trace gases to the atmosphere, though a close examination of the environment, sampling protocol, and measurement goals is needed to maximize their potential.

■ ASSOCIATED CONTENT

Supporting Information

Additional information on the flight and meteorology details of individual flights, the larger meteorological context between flights, and additional notes on the Gaussian plume modeling are included. The Supporting Information is available free of charge on the ACS Publications website at DOI: 10.1021/acs.est.5b00705.

■ AUTHOR INFORMATION

Corresponding Author

*Phone: (609)- 258-5037; e-mail: mzondlo@princeton.edu.

Notes

The authors declare no competing financial interest.

■ ACKNOWLEDGMENTS

We acknowledge Josh DiGangi, Levi Stanton, Kang Sun, and David Miller of Princeton University for the sensor development, deployment, and analyses. In addition, we acknowledge Xin Lan and Robert Talbot at the University of Houston for the mobile methane measurements. We acknowledge Dave Schaefer for his very able direction of all aircraft operations. We also very much appreciate the permission of the site operator and local residents, landowners, and airfield operators to fly the aircraft over their properties. We acknowledge Jenna Granstra from the URS Corporation for the TCEQ meteorological data. This work was financially supported by the Environmental Defense Fund (EDF) and NSF EEC-0540832. The authors thank three anonymous reviewers for constructive comments on the manuscript.

■ REFERENCES

(1) Brandt, A. R.; Heath, G. A.; Kort, E. A.; Pétron, G.; Jordaan, S. M.; Tans, P.; Wilcox, J.; Gopstein, A. M.; Arent, D.; Wofsy, S.; et al. Methane leaks from North American natural gas systems. *Science* **2014**, DOI: 10.1126/science.1247045.

(2) Allen, D. T.; Torres, V. M.; Thomas, J.; Sullivan, D. W.; Harrison, M.; Hendler, A.; Herndon, S. C.; Kolb, C. E.; Fraser, M. P.; Hill, A. D.; et al. Measurements of methane emissions at natural gas production sites in the United States. *Proc. Natl. Acad. Sci. U. S. A.* **2013**, DOI: 10.1073/pnas.1304880110.

(3) Brantley, H. L.; Thoma, E. D.; Squier, W. C.; Guven, B. B.; Lyon, D. Assessment of methane emissions from oil and gas production pads using mobile measurements. *Environ. Sci. Technol.* **2014**, DOI: 10.1021/es503070q.

(4) Lan, X.; Talbot, R.; Laine, P.; Torres, A. Characterizing fugitive methane emissions in the Barnett Shale area using a mobile laboratory. *Environ. Sci. Technol.* **2015**, DOI: 10.1021/es5063055.

(5) Mays, K. L.; Shepson, P. B.; Stirm, B. H.; Karion, A.; Sweeney, C.; Gurney, K. R. Aircraft-based measurements of the carbon footprint of Indianapolis. *Environ. Sci. Technol.* **2009**, DOI: 10.1021/es901326b.

(6) Caulton, D.; Shepson, P. B.; Cambaliza, M. O. L.; McCabe, D.; Baum, E.; Stirm, B. H. Methane destruction efficiency of natural gas flares associated with shale formation wells. *Environ. Sci. Technol.* **2014**, DOI: 10.1021/es500511w.

(7) Caulton, D. R.; Shepson, P. B.; Santoro, R. L.; Sparks, J. P.; Howarth, R. W.; Ingraffea, A. R.; Cambaliza, M. O. L.; Sweeney, C.; Karion, A.; Davis, K. J.; et al. Toward a better understanding and quantification of methane emissions from shale gas development. *Proc. Natl. Acad. Sci. U. S. A.* **2014**, DOI: 10.1073/pnas.131654611.

(8) Khan, A.; Schaefer, D.; Tao, L.; Miller, D. J.; Sun, K.; Zondlo, M. A.; Harrison, W. A.; Roscoe, B.; Lary, D. J. Low power greenhouse gas sensors for unmanned aerial vehicles. *Remote Sens.* **2012**, DOI: 10.3390/rs4051355.

(9) Harris, R.; Alvarez, R. A.; Lyon, D.; Hamburg, S. P.; Nelson, D.; Zavala-Araiza, D. Using multi-scale measurements to improve methane emissions estimates from oil and gas operations in the Barnett Shale region, Texas *Environ. Sci. Technol.* **2015**, DOI: 10.1021/es506359c.

(10) Johnson, D. R.; Covington, A. N.; Clark, N. N. Methane emissions from leak and loss audits of natural gas compressor stations and storage facilities. *Environ. Sci. Technol.* **2015**, DOI: 10.1021/es506163m.

(11) U.S. Energy Information Administration. Natural gas compressor stations on the interstate pipeline network: Developments since 1996. Office of Oil and Gas, http://www.eia.gov/pub/oil_gas/natural_gas/analysis_publications/ngcompressor/ngcompressor.pdf.

(12) Myers, D. E. Interpolation and estimation with spatially located data. *Chemom. Intell. Lab. Syst.* **1991**, *11*, 209–228.

(13) Arya, S. P. *Air Pollution Meteorology and Disperion*; Oxford University Press, 1999.

(14) Pasquill, F. The estimation of the dispersion of windborne material. *Meteorol. Mag.* **1961**, *90*, 33–49.

(15) *User's Guide for the Industrial Source Complex (ISC3) Dispersion Models Volume II—Description of Model Algorithms*; United States Environmental Protection Agency, 1995.
(16) McDermitt, D.; Burba, G.; Xu, L.; Anderson, T.; Komissarov, A.; Riensche, B.; Schedbauer, J.; Starr, G.; Zona, D.; Oechel, W.; et al. A new low-power, open-path instrument for measuring methane flux by eddy covariance. *Appl. Phys. B: Lasers Opt.* **2012**, DOI: 10.1007/s00340-010-4307-0.
(17) Karion, A.; Sweeney, C.; Pétron, G.; Frost, G.; Hardesty, R. M.; Kofler, J.; Miller, B. R.; Newberger, T.; Wolter, S.; Banta, R.; et al. Methane emissions estimate from airborne measurements over a western United States natural gas field, *Geophys. Res. Lett.* **2013**, *40*, DOI: 10.1002/grl.50811.
(18) Pecha, P.; Hofman, R. Fitting of segmented Gaussian plume model predictions on measured data. *Proceedings of the 22th European Simulation and Modelling Conference ESM'2008.* **2008**, 544−548.
(19) Krysta, M.; Bocquet, M.; Sportisse, B.; Isnard, O. Data assimilation for short-range dispersion of radionuclides: An application to wind tunnel data. *Atmos. Environ.* **2006**, *40* (38), 7267−7279.

DOI: 10.1021/acs.est.5b00705
Environ. Sci. Technol. 2015, 49, 7896−7903